Delay-Phase Precoding to Alleviate Beam Defocus Effect for Circular Arrays

Zidong Wu, and Linglong Dai, *Fellow, IEEE*

Department of Electronic Engineering, Tsinghua University,
Beijing National Research Center for Information Science and Technology (BNRist), Beijing 100084, China
Email: wuzd19@mails.tsinghua.edu.cn, daill@tsinghua.edu.cn

***Abstract*—Millimeter-wave (mmWave) and terahertz (THz) communications with hybrid precoding architectures have been regarded as energy-efficient methods to fulfill the vision of high-speed transmissions for 6G communications. Benefiting from the advantages of providing a wide scan range and uniform array pattern, uniform circular array (UCA) has attracted much attention. However, the growing bandwidth of mmWave and THz communications require frequency-independent phase shifts to perform beamforming, which can not be perfectly realized through frequency-independent phase shifters (PSs) in hybrid precoding schemes. This mismatch causes the beam defocus effect in UCA systems, where high-gain beams disappear at non-central frequencies. In this paper, we first investigate the characteristics of the beam defocus effect distinguishing from beam split effect in uniform linear array (ULA) systems. The beam pattern of UCA in both frequency and angular domain is analyzed, characterizing the beamforming loss caused by beam defocus effect. Then, the delay-phase precoding (DPP) architecture leveraging true-time-delay (TTD) is employed to mitigate the beam defocus effect. Finally, performance analysis and simulations are provided to evaluate the performance improvement with DPP architectures.**

I. Introduction

To meet the ever-increasing growth of data transmission demand, high-frequency bands such as millimeter-wave (mmWave) and terahertz (THz) are promising to provide abundant spectrum resources for future 6G communications. To combat the high propagation attenuation in high-frequency bands, massive multiple-input multiple-output (MIMO) with the hybrid precoding architecture has been regarded as an energy-efficient way to form high-gain directional beams to extend communication coverage ability [1].

However, although the hybrid precoding architectures have worked well in narrowband communications, they will experience the beam split effect which worsens the beamforming gain in wideband communications. In wideband communications, the required phase shifts to form constructive interference are frequency-dependent, while phase shifters (PSs) in hybrid precoding could only generate the same phase shifts at different frequencies, i.e. frequency-independent phase shifts. This mismatch results in beams at non-central frequencies being squinted from the desired direction, which was termed the *beam split* effect in THz communications [2].

Most of existing works aiming to solve the beam split effect in hybrid precoding designs were restricted to uniform linear arrays (ULAs). Nevertheless, the effective array aperture of ULA dramatically reduces at large angles of incidence, resulting in a distorted beam pattern and reduced array gain. Due to the feature of axial symmetry, the uniform circular array (UCA) has been regarded as a feasible solution to providing 360° coverage and uniform beam pattern at varying azimuth angles [3]. In this paper, we reveal that due to the variation of the array geometry from ULA to UCA, the beam split effect is not feasible to characterize wideband UCA systems anymore. Instead, we reveal that a new effect different from beam split effect appears in UCA systems. To the best of our knowledge, the mechanism of this effect and the corresponding solution have not been investigated in existing works.

In this paper, we first reveal that the mismatch of generated frequency-independent phase shifts and required frequency-dependent phase shifts will not necessarily cause split high-gain beams. In UCA systems, high-gain beams at non-central frequencies may totally disappear in any direction due to non-ideal phase shifts, which is fundamentally different from the beam split effect in ULA systems. We term this effect the *beam defocus* effect. Then, the mechanism of the beam defocus effect is investigated, where the array pattern in both frequency domain and angular domain is characterized. To mitigate the beam defocus effect, the delay-phase precoding (DPP) architecture is employed, and the corresponding precoding algorithm is proposed. Analysis and simulations are provided to verify the effectiveness of the employed DPP method.

The remainder of the paper is organized as follows. Section II introduces the wideband UCA system model. Section III investigates the beam defocus effect. The DPP architecture is employed in Section IV, and performance analysis is provided in Section V. Simulation results are shown in Section VI, and conclusions are drawn in Section VII.

II. System Model

We consider a mmWave wideband communication system, where the hybrid precoding scheme is adopted. The base station (BS) equipped with an N-element UCA aims to serve users with N_{r}-element ULAs, where users are assumed to be in the same plane of UCA as shown in Fig. 1. The BS employs N_{RF} RF chains, each of which connects to all antennas. To harvest the spatial multiplexing gain, multiple data streams are transmitted, satisfying $N_{\mathrm{s}} \leq N_{\mathrm{RF}} \leq N$. We assume $N_{\mathrm{s}} = N_{\mathrm{RF}} \ll N$ in this paper for ease of illustration. The orthogonal frequency division multiplexing (OFDM) model with M subcarriers is employed and the bandwidth is set to B. The central frequency is denoted by f_c and the m^{th}

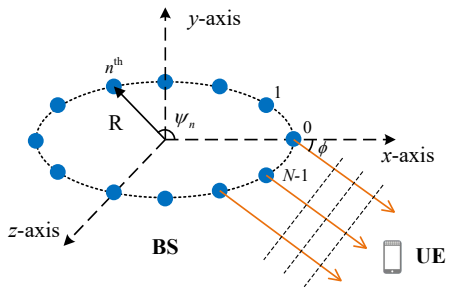

Fig. 1. The geometrical relationship between the UCA at BS and users in the same plane.

subcarrier is denoted by $f_m = f_c + \frac{B(2m-1-M)}{2M}$. Thus, the received signal at the m^{th} subcarrier could be expressed as

$$\mathbf{y}_m = \rho \mathbf{H}_m^H \mathbf{F}_{\text{A}} \mathbf{F}_{\text{D},m} \mathbf{s}_m + \mathbf{n}_m, \tag{1}$$

where $\mathbf{H}_m \in \mathbb{C}^{N \times N_{\text{r}}}$ denotes the channel, $\mathbf{F}_{\text{A}} \in \mathbb{C}^{N \times N_{\text{s}}}$ and $\mathbf{F}_{\text{D},m} \in \mathbb{C}^{N_{\text{s}} \times N_{\text{s}}}$ denote the analog precoder and digital precoder, respectively. Note that since the digital precoder is conducted before digital-to-analog converters (DACs), it could be performed subcarrier by subcarrier and therefore is frequency-dependent. On the contrary, the analog precoder implemented by PSs introduces frequency-invariant phase shifts at different frequencies. Thus, $\mathbf{F}_{\text{A}}$ is frequency-independent with additional constraints $|[\mathbf{F}_{\text{A}}]_{i,j}| = \frac{1}{\sqrt{N}}$. The transmitted signal $\mathbf{s}_m \in \mathbb{C}^{N_{\text{s}} \times 1}$ and noise $\mathbf{n}_m \in \mathbb{C}^{N_{\text{r}} \times 1}$ follow $\mathbb{E}(\mathbf{s}_m \mathbf{s}_m^H) = \frac{1}{N_{\text{s}}} \mathbf{I}_{N_{\text{s}}}$ and $\mathbf{n}_m \sim \mathcal{CN}(0, \sigma_n^2 \mathbf{I})$, respectively.

Adopting the classical Saleh-Valenzuela channel model [4], the wireless channel could be written as

$$\mathbf{H}_m = \sqrt{\frac{N}{L}} \sum_{l=1}^{L} g_l e^{-j2\pi\tau_l f_m} \mathbf{a}_m(\phi_l) \bar{\mathbf{a}}_m^H(\varphi_l), \tag{2}$$

where $\mathbf{a}_m(\cdot)$ and $\bar{\mathbf{a}}_m(\cdot)$ denote the beam steering vectors at the BS and user, respectively. Notation g_l, τ_l, ϕ_l, and φ_l denote the path gain, delay, angle of departure and arrival of the l^{th} path, respectively. The expression of beam steering vector can be viewed as frequency response vectors of impinging waves, which are highly dependent on the array geometry. As shown in Fig. 1, beam steering vector of UCA can be written as [3]

$$\mathbf{a}_m(\phi) = \frac{1}{\sqrt{N}} \left[e^{j\eta_m \cos(\phi - \psi_0)}, \cdots, e^{j\eta_m \cos(\phi - \psi_{N-1})} \right]^T, \tag{3}$$

where $\eta_m = \frac{2\pi R}{c} f_m$ for $m = 1, 2, \cdots, M$ and $\psi_n = \frac{2\pi n}{N}$ for $n = 0, 1, \cdots, N-1$. While at the user side, ULA is employed to fulfill the more strict requirements on the array deployment, where the ULA's beam steering vector could be expressed as

$$\bar{\mathbf{a}}_m(\varphi) = \frac{1}{\sqrt{N_{\text{r}}}} \left[1, e^{j\frac{2\pi d f_m}{c} \sin\varphi}, \cdots, e^{j\frac{2\pi(N-1) d f_m}{c} \sin\varphi} \right]^T. \tag{4}$$

III. Beam Defocus Effect in UCA Systems

In hybrid precoding architectures, the analog precoder and digital precoder are combined to generate directional beams and mitigate interferences to simultaneously harvest the spatial multiplexing gain and beamforming gain [1]. Specifically, analog precoding is aimed at forming high-gain beams by performing constructive interference in desired directions. To achieve this goal, PSs are elaborately designed to compensate for the phase differences between different antennas. It has been revealed that PSs could only generate frequency-independent phases [2]. However, note that phase differences between different antennas change with frequency in beam steering vectors (3) and (4). Therefore, to perfectly compensate for the phase differences between antennas, the required phase shifts also need to be frequency-dependent. This mismatch will result in the degraded beamforming gain in wideband systems.

Recently, it has been demonstrated that this mismatch has given rise to the beam split effect in ULA systems [2]. With the beam split effect, the single beam will split into beams pointing in different directions at different frequencies, which dramatically decreases the beamforming gain. Nevertheless, the beam split effect is only restricted to ULA systems. As the array geometry varies from linear to circular, a different effect will engage, which shall be discussed as follows.

Lemma 1. If the frequency-independent beam steering vector $\mathbf{a}_c(\phi)$ is employed to perform beamforming, the achieved beamforming gain at f_m in desired direction ϕ follows

$$\begin{aligned} G_m(\mathbf{a}_c(\phi), \phi) &= \left| \mathbf{a}_m^H(\phi) \mathbf{a}_c(\phi) \right| \\ &= \left| \frac{1}{N} \sum_{n=0}^{N-1} e^{-j(\eta_m - \eta_c)\cos(\phi - \psi_n)} \right| \\ &\approx |J_0(\eta_m - \eta_c)| = \left| J_0\left(\frac{2\pi R (f_m - f_c)}{c} \right) \right|, \end{aligned} \tag{5}$$

where $J_0(\cdot)$ denotes the zero-order Bessel function of the first kind, $\eta_m = \frac{2\pi R}{c} f_m$ and $\eta_c = \frac{2\pi R}{c} f_c$.

Proof. The proof starts from the Jacobi-Anger expansion of Bessel functions [5], which is written as

$$e^{j\beta\cos\gamma} = \sum_{s=-\infty}^{\infty} j^s J_s(\beta) e^{js\gamma}, \tag{6}$$

where $J_s(\cdot)$ denotes the s-order Bessel function. By substituting (6) into (5) and exchanging the summations, we obtain

$$G_m(\mathbf{a}_c(\phi), \phi) \overset{(a)}{=} \frac{1}{N} \left| \sum_{s=-\infty}^{\infty} j^s J_s(\eta_c - \eta_m) e^{js\phi} \sum_{n=0}^{N-1} e^{-js\psi_n} \right|. \tag{7}$$

Then, the summation over n could be expressed as the piecewise function as

$$\sum_{n=0}^{N-1} e^{-js\psi_n} = \begin{cases} N, & s = N \cdot t, t \in \mathbb{Z} \\ 0, & s \neq N \cdot t, t \in \mathbb{Z}. \end{cases} \tag{8}$$

The piecewise function equals zero except on integral multiples of N. We assume that N is large enough, which has been a common assumption in the research of UCA systems [6]. Then, the value of $|J_{|s|}(x)|$ could be assumed negligible for large s [6]. Therefore, $|J_{|s|}(x)| \approx 0$ could be obtained for

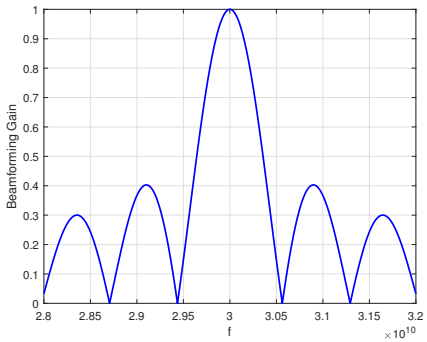

Fig. 2. The beamforming gain achieved with frequency-independent phase shifts at different frequencies.

$s = N \cdot t$ with $t \neq 0$ and large N. Finally, the summation could obtain an accurate approximation with $s = 0$, written as

$$G_m(\mathbf{a}_c(\phi), \phi) \approx |J_0(\eta_c - \eta_m)| = |J_0(\eta_m - \eta_c)|, \quad (9)$$

which completes the proof. ■

Remark 1. This lemma characterizes the beamforming loss resulting from the mismatch of generated frequency-independent phase shifts and required frequency-dependent phase shifts in the frequency domain. According to the property of $J_0(x)$, the beamforming gain employing PSs could only achieve the maximum when $f_m = f_c$, i.e. at the central frequency. Perfect constructive interferences could not form at any subcarrier other than the central frequency, introducing undesired beamforming loss across the wide bandwidth. In addition, we note that the beamforming gain is independent of ϕ, which results from the axial symmetry of UCA.

To demonstrate how serious the loss is, the beamforming gain at different frequencies is plotted in Fig. 2, with $f_c = 30$ GHz and $B = 4$ GHz. The BS is equipped with a 256-element half-wavelength spaced UCA. It is shown that the optimal beamforming could only be achieved at the central frequency, which is consistent with **Lemma 1**. According to the overall downtrend of $|J_0(x)|$, a larger bandwidth will overall result in a more severe beamforming loss, indicating that wideband communications with UCA will suffer from severe loss.

Although this phenomenon may seem very much like the beam split effect for ULA, we shall illustrate the distinction of this phenomenon fundamentally different from the beam split effect as follows.

Lemma 2. If the frequency-independent beam steering vector $\mathbf{a}_c(\phi_0)$ is employed, the achieved beamforming gain at frequency f_m in any direction ϕ could be expressed as

$$G_m(\mathbf{a}_c(\phi_0), \phi) = \left|\mathbf{a}_m^H(\phi)\mathbf{a}_c(\phi_0)\right| \approx |J_0(\xi)|, \quad (10)$$

where parameter ξ is defined as

$$\xi = \sqrt{\eta_m^2 + \eta_c^2 - 2\eta_m\eta_c\cos(\phi - \phi_0)}. \quad (11)$$

Proof. The proof can be seen in [7] Appendix A. ■

This lemma characterizes the beam pattern in the angular domain. According to the property of $J_0(\cdot)$, the beamforming gain could only achieve maximum when $\xi = 0$, i.e. $f_m = f_c$ and $\phi = \phi_0$. Note that if $\phi = \phi_0$ is assumed, the result in **Lemma 2** will degrade into **Lemma 1**. Therefore, **Lemma 2** depicts a more general case where ϕ can be arbitrarily selected. At frequency $f_m \neq f_c$, beamforming gain could not reach 1 in any direction. As a consequence, high-gain beams could not form except at the central frequency. This phenomenon is fundamentally different from the beam split effect with ULA, where high-gain beams split into separated physical directions but remain the optimal beamforming gain.

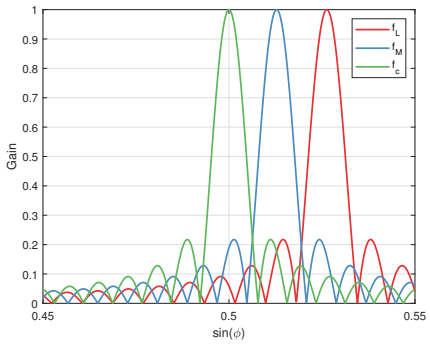

(a) Beam Split Effect

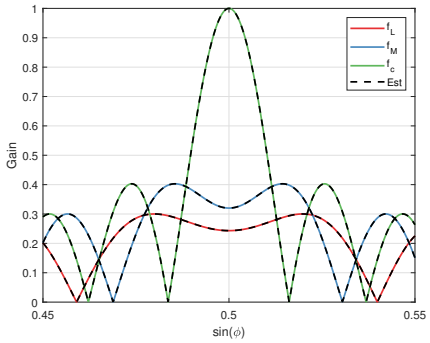

(b) Beam Defocus Effect

Fig. 3. Comparison of beam split effect and beam defocus effect in the angular domain. Both systems are designed to generate beams towards $\sin(\phi) = 0.5$ at central frequency. $f_L = 28.5$ GHz and $f_c = 30$ GHz denote the lowest frequency and central frequency, while f_M is defined as $f_M = \frac{f_L + f_c}{2}$.

To clearly illustrate their differences, a comparison of the beam pattern in the angular domain is shown in Fig. 3, where different colored lines represent the beam pattern at different frequencies. Specifically, the high-gain beams slightly squint from the desired direction but retain the same beam pattern in the beam split effect, as shown in Fig. 3(a). On the contrary, the beam pattern is severely distorted at non-central frequencies in Fig. 3(b). The high-gain beams no longer exist in any direction, which is consistent with **Lemma 2**. Since it is similar to the defocus phenomenon in photography where the photo becomes blurred due to *failed focusing*, we name it the *beam defocus effect*. In addition, the colored solid lines in Fig. 3(b) denote the accurately calculated beamforming gain while the black dashed lines denote the estimated beamforming gain with (10). The consistency of the solid and dashed lines indicates that (10) could achieve accurate estimations.

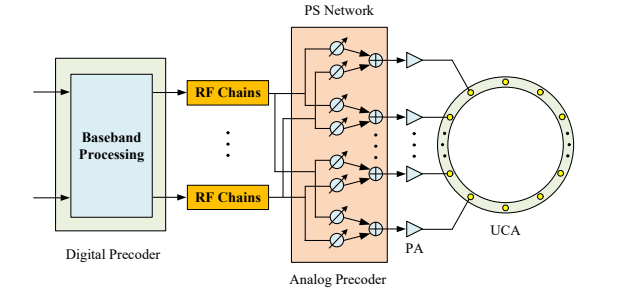

(a) Classical Hybrid Precoding Architecture

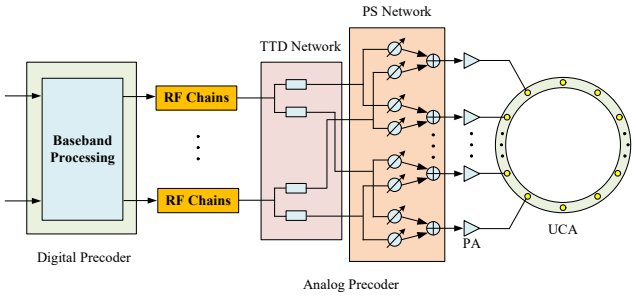

(b) Delay-Phase Precoding Architecture

Fig. 4. Comparison of hybrid precoding architecture and DPP architecture.

IV. DPP Architecture to Alleviate the Beam Defocus Effect

As discussed in previous sections, severe beamforming loss will be introduced in classical PS-based hybrid precoding architectures due to the beam defocus effect, which remarkably worsens the received signal quality across the bandwidth.

To break the hardware constraints of PS which could only generate frequency-independent phase shifts, true-time-delays (TTDs) have been incorporated into hybrid precoding architectures [2]. In this architecture, delays of TTDs and phase shifts of PSs are combined to produce frequency-dependent phase shifts to cope with the beam split effect in ULA systems, which is also called the DPP architecture.

Noting that despite different manifestations, beam split effect and beam defocus effect share the same root cause, that is the mismatch of the generated frequency-independent phase shifts and required frequency-dependent phase shifts. Inspired by this discovery, we propose to generalize the DPP architecture originally employed in ULA systems into UCA systems to alleviate the beam defocus effect. Different from the classical hybrid precoding architecture in Fig. 4(a), the DPP architecture additionally introduces a TTD network to generate frequency-dependent phase shifts, as shown in Fig. 4(b). In this paper, we assume each RF chain connects to K TTDs and each TTD connects to $P = \frac{N}{K}$ antennas in a sub-connected manner.

Based on the DPP architecture, the TTD-PS analog precoder corresponding to the l^{th} channel component is expressed as

$$\mathbf{b}_{m,l} = \text{blkdiag}(\mathbf{F}_l)\mathbf{p}_{l,m}, \tag{12}$$

where $\mathbf{F}_l = [\mathbf{f}_{l,1}, \mathbf{f}_{l,2}, \cdots, \mathbf{f}_{l,K}]$ and $\mathbf{p}_{l,m} \in \mathbb{C}^{K\times 1}$ represents phase shifts generated by K TTDs. Note that each column of $\mathbf{F}_l$ corresponds to the frequency-independent phase shifts linking to one TTD, the element of which has the constant modulus constraint $|[\mathbf{f}_{l,i}]_j| = \frac{1}{\sqrt{N}}$. Roughly speaking, phase shifts generated by TTDs can be linear to frequency[1].

Then, the analog precoding design could be decomposed into two components, i.e. frequency-independent $\mathbf{f}_{l,i}$ and frequency-dependent $\mathbf{p}_{l,m}$. Therefore, the objective of analog precoding is to maximize the beamforming gain with $\mathbf{b}_{m,l}$.

Note that PSs work well in narrowband systems but fail to meet the frequency-dependent phase shift requirements in wideband systems. A natural method is first designing PSs to align the beam towards the desired direction at central frequency, like in narrowband systems. Then, TTDs are designed to compensate for frequency-dependent residual components in each subarray, aiming to mitigate the beam defocus effect. Following this method, $\mathbf{F}_l$ could be designed as

$$\mathbf{F}_l = [\mathbf{a}_c(\phi_l)_1, \mathbf{a}_c(\phi_l)_2, \cdots, \mathbf{a}_c(\phi_l)_K], \tag{13}$$

where $\mathbf{a}_c(\phi_l)_i \in \mathbb{C}^{P\times 1}$ denotes the i^{th} subvector of $\mathbf{a}_c(\phi_l)$. Then, the delays of TTDs could be obtained as follows.

Lemma 3. Optimal designed $\mathbf{p}_{l,m}$ compensating for frequency-dependent residuals of l^{th} path can be written as

$$[\mathbf{p}_{l,m}]_k = \exp\left\{ j\frac{2\pi R}{c}(f_m - f_c)\cos\left(\phi_l - \bar{\theta}_k\right)\right\}, \tag{14}$$

where $\bar{\theta}_k = \frac{2\pi k}{K} + \frac{(P-1)\pi}{N}$, $[\mathbf{p}_{l,m}]_k$ denotes the k^{th} element of $\mathbf{p}_{l,m}$. The corresponding beamforming gain follows

$$G_m(\mathbf{b}_{m,l}, \phi_l) \approx \frac{1}{P}\sum_{i=0}^{P-1} J_0(R_i), \tag{15}$$

where $R_i = \frac{2\sqrt{2}\pi R}{c}(f_m - f_c)\sqrt{1 - \cos\left(\frac{(2i+1)\pi}{N} - \frac{\pi}{K}\right)}$.

Proof. The proof can be seen in [7] Appendix B. ■

The result is consistent with the intuition that one TTD should compensate for the frequency-dependent residuals *at the center of each subarray* to obtain a good compensation performance. Despite the similar usage methods of TTD networks, the possibility of TTD being applied in different array geometries and the principle of compensating residuals at the center of subarrays are first illustrated. In addition, we find that the assumption of delays linear to subarray indices is only applicable in ULA systems, and should be relaxed for different array geometries. Through this lemma, we can see that the beamforming gain after introducing TTDs is highly dependent on the choice of K. Due to the difficulty in extracting the relationship between beamforming gain and K, we seek a more succinct expression of beamforming gain as follows.

Corollary 1. Assuming a large K, the beamforming gain with DPP architectures obtained in (15) could be simplified as

$$G_m(\mathbf{b}_{m,l}, \phi_l) \approx \left| {}_1F_2\left(\frac{1}{2}; 1, \frac{3}{2}; -\frac{a^2}{4}\right)\right|, \tag{16}$$

[1]It is worth noting that a pure delay of TTD results in phase shifts in proportion to frequency. Nevertheless, the frequency-independent term could be realized through PSs. Therefore, we relax the constraint of TTDs from in proportion to frequency to linear to frequency here.

where the notation ${}_1F_2$ represents the generalized hypergeometric function and $a = \frac{2\pi^2 R}{cK}(f_m - f_c)$.

Proof. The proof can be seen in [7] Appendix C. ■

Although the special function ${}_1F_2(\cdot)$ in (16) seems complicated, it is still a one-variable function over a. According to the overall downtrend of ${}_1F_2(\frac{1}{2}; 1, \frac{3}{2}; -\frac{x^2}{4})$ against x, we can sketchily conclude that a larger number of TTDs will contribute to an increased beamforming gain, which also makes intuitive sense.

Next, we shall introduce the whole precoding algorithm consisting of digital precoder, analog precoder implemented by TTDs, and analog precoder implemented by PSs. Based on DPP architectures, the received signal can be rewritten as

$$\mathbf{y}_m = \sqrt{\rho}\mathbf{H}_m^H \mathbf{F}_{\mathrm{A}}^{\mathrm{PS}} \mathbf{F}_{\mathrm{A},m}^{\mathrm{TTD}} \mathbf{F}_{\mathrm{D},m} \mathbf{s}_m + \mathbf{n}_m, \tag{17}$$

where $\mathbf{F}_{\mathrm{A}}^{\mathrm{PS}}$ and $\mathbf{F}_{\mathrm{A},m}^{\mathrm{TTD}}$ denote the analog precoding corresponding to the PS network and TTD network, respectively. According to the functional principle of TTDs, the phase shift generated by TTD has to be strictly proportional to frequency, written as $-2\pi f_m t$ where t denotes the delay. Noticing that the optimal phase shifts required for the k^{th} TTD in equation (14) have two separated components, written as

$$\angle[\mathbf{p}_{l,m}]_k^* = -\frac{2\pi R}{c}\cos\left(\phi_l - \bar{\theta}_k\right) f_c + \frac{2\pi R}{c}\cos\left(\phi_l - \bar{\theta}_k\right) f_m, \tag{18}$$

where the former is frequency-independent while the latter is exactly proportional to frequency f_m. Therefore, we can realize these two components with PS and TTD, respectively. Thus, the required time delay for the k^{th} TDD corresponding to the l^{th} path has to satisfy

$$-2\pi f_m t_{l,k} = \frac{2\pi R}{c}\cos\left(\phi_l - \bar{\theta}_k\right) f_m. \tag{19}$$

Then, we can obtain $t_{l,k} = -\frac{R}{c}\cos\left(\phi_l - \bar{\theta}_k\right)$. In addition, since TTD has an additional constraint $t_l > 0$, a global time delay needs to be added to all TTDs without influencing the beamforming performance, written as

$$\widetilde{t}_{l,k} = \frac{R}{c}\left(1 - \cos\left(\phi_l - \bar{\theta}_k\right)\right) \geq 0. \tag{20}$$

Finally, the TTD-based analog precoder can be written as

$$\widetilde{\mathbf{p}}_{l,m} = [e^{-2\pi f_m \widetilde{t}_{l,1}}, e^{-2\pi f_m \widetilde{t}_{l,2}}, \cdots, e^{-2\pi f_m \widetilde{t}_{l,K}}]^T. \tag{21}$$

So far, the frequency-dependent component of phase shifts has been realized. After combining the frequency-independent component in (18) into the original analog precoder $\mathbf{F}_l$ in (13), the modified PS-based analog precoder $\widetilde{\mathbf{F}}_l$ can be written as

$$\widetilde{\mathbf{f}}_{l,k} = \mathbf{a}_c(\phi_l)_k e^{-\frac{2\pi R}{c}\cos\left(\phi_l - \bar{\theta}_k\right) f_c}, \tag{22}$$

where $\widetilde{\mathbf{f}}_{l,k}$ denotes the k^{th} column of $\widetilde{\mathbf{F}}_l$. Finally, $\mathbf{F}_{\mathrm{A}}^{\mathrm{TTD}}$ and $\mathbf{F}_{\mathrm{A}}^{\mathrm{PS}}$ can be constructed with $\widetilde{\mathbf{p}}_{l,m}$ and $\widetilde{\mathbf{F}}_l$, respectively.

The proposed DPP algorithm is summarized in **Algorithm 1**. We first rearrange the channel components in descending order, trying to deal with the most significant channel components, as shown in line 1. Following the same procedure above, the PS-based analog precoder can be constructed as lines 3, 5, and 8, and the TDD-based analog precoder can be constructed as lines 6 and 9. Then, by concatenating the derived precoders for each RF chain, the analog precoder can be obtained in lines 11-12. Finally, we can follow the classical water-filling procedure, using the singular value decomposition (SVD) to obtain the digital precoder, as shown in lines 13-14.

Algorithm 1 DPP algorithm for UCA.

Input: Channel $\mathbf{H}_m$ and angles ϕ_l
Output: Analog and digital precoders $\mathbf{F}_{\mathrm{A}}^{\mathrm{PS}}$, $\mathbf{F}_{\mathrm{A},m}^{\mathrm{TTD}}$, $\mathbf{F}_{\mathrm{D},m}$

1: Rearrange the order of channel components $|g_1| \geq |g_2| \geq \cdots \geq |g_{\mathrm{RF}}|$ and obtain corresponding $\{\phi_1, \cdots, \phi_{\mathrm{RF}}\}$;
2: **for** $l = 1, 2, \cdots, N_{\mathrm{RF}}$ **do**
3: Construct the beam steering vector $\mathbf{a}_c(\phi_l)$ by (3);
4: **for** $k = 1, 2, \cdots, K$ **do**
5: Determine phase shifts of PS $\widetilde{\mathbf{f}}_{l,k}$ by (22);
6: Determine delay for k^{th} TTD $\widetilde{t}_{l,k}$ by (20);
7: **end for**
8: Construct $\widetilde{\mathbf{F}}_l = [\widetilde{\mathbf{f}}_{l,1}, \cdots, \widetilde{\mathbf{f}}_{l,K}]$;
9: Construct $\widetilde{\mathbf{p}}_{l,m} = [e^{-j2\pi f_m \widetilde{t}_{l,1}}, \cdots, e^{-j2\pi f_m \widetilde{t}_{l,K}}]^T$;
10: **end for**
11: Construct $\mathbf{F}_{\mathrm{A}}^{\mathrm{PS}} = \left[\mathrm{blkdiag}(\widetilde{\mathbf{F}}_1), \cdots, \mathrm{blkdiag}(\widetilde{\mathbf{F}}_{N_{\mathrm{RF}}})\right]$;
12: Construct $\mathbf{F}_{\mathrm{A},m}^{\mathrm{TTD}} = \mathrm{blkdiag}\left([\widetilde{\mathbf{p}}_{1,m}, \cdots, \widetilde{\mathbf{p}}_{N_{\mathrm{RF}},m}]\right)$;
13: Obtain the equivalent channel $\mathbf{H}_{\mathrm{eq},m}^H = \mathbf{H}_m^H \mathbf{F}_{\mathrm{A}}^{\mathrm{PS}} \mathbf{F}_{\mathrm{A},m}^{\mathrm{TTD}}$ with $\mathbf{H}_{\mathrm{eq},m}^H = \mathbf{U}_{\mathrm{eq},m}\mathbf{\Sigma}_{\mathrm{eq},m}\mathbf{V}_{\mathrm{eq},m}^H$;
14: Determine the digital precoder $\mathbf{F}_{\mathrm{D},m} = \mathbf{V}_{\mathrm{eq},m}\mathbf{\Lambda}$;
15: **return** $\mathbf{F}_{\mathrm{A}}^{\mathrm{PS}}$, $\mathbf{F}_{\mathrm{A},m}^{\mathrm{TTD}}$ and $\mathbf{F}_{\mathrm{D},m}$.

V. System Performance Analysis

The spectrum efficiency at the m^{th} subcarrier can be expressed as

$$R_m = \log_2\left(\left|\mathbf{I} + \frac{\rho}{N_s\sigma_n^2}\mathbf{H}_m^H \mathbf{F}_{\mathrm{A}} \mathbf{F}_{\mathrm{D},m} \mathbf{F}_{\mathrm{D},m}^H \mathbf{F}_{\mathrm{A}}^H \mathbf{H}_m\right|\right), \tag{23}$$

where $\mathbf{F}_{\mathrm{A}}$ can be further decomposed as $\mathbf{F}_{\mathrm{A}} = \mathbf{F}_{\mathrm{A}}^{\mathrm{PS}}\mathbf{F}_{\mathrm{A},m}^{\mathrm{TTD}}$. According to [4], when the number of RF chains exceeds the number of resolvable paths, the spatial multiplexing gain could be fully harvested. Then, by assuming SVD of the channel $\mathbf{H}_m^H = \mathbf{U}_m\mathbf{\Sigma}_m\mathbf{V}_m^H$ and extracting the significant sub-channels as $\widetilde{\mathbf{\Sigma}}_m = [\mathbf{\Sigma}_m]_{1:N_{\mathrm{s}},1:N_{\mathrm{s}}}$ and $\widetilde{\mathbf{V}}_m = [\widetilde{\mathbf{V}}_m]_{:,1:N_{\mathrm{s}}}$, the spectrum efficiency can be reformulated into

$$R_m = \log_2\left(\left|\mathbf{I} + \frac{\rho}{N_s\sigma_n^2}\widetilde{\mathbf{\Sigma}}_m^2 \mathbf{V}_{m,\mathrm{eq}}^H \mathbf{V}_{m,\mathrm{eq}}\right|\right), \tag{24}$$

where $\mathbf{V}_{m,\mathrm{eq}} = \mathbf{F}_{\mathrm{D},m}^H \mathbf{F}_{\mathrm{A},m}^{\mathrm{TTD}H} \mathbf{F}_{\mathrm{A}}^{\mathrm{PS}H} \widetilde{\mathbf{V}}_m$. We adopt the linear transformation in [4] which reformulates the unitary matrix $\widetilde{\mathbf{V}}_m$ with a list of orthogonal steering vectors, expressed as

$$\widetilde{\mathbf{V}}_m \approx \mathbf{A}_{\mathrm{t},m}\mathbf{F}_{\mathrm{D,m}}^{\mathrm{opt}}, \tag{25}$$

where $\mathbf{A}_{\mathrm{t},m} = [\mathbf{a}_m(\phi_1), \cdots, \mathbf{a}_m(\phi_{N_{\mathrm{s}}})]$ and $\mathbf{F}_{\mathrm{D,m}}^{\mathrm{opt}}$ denote the optimal digital precoder maximizing the spectrum efficiency [4]. When the number of antennas tends to infinity, the steering vectors could form an orthogonal basis, indicating that

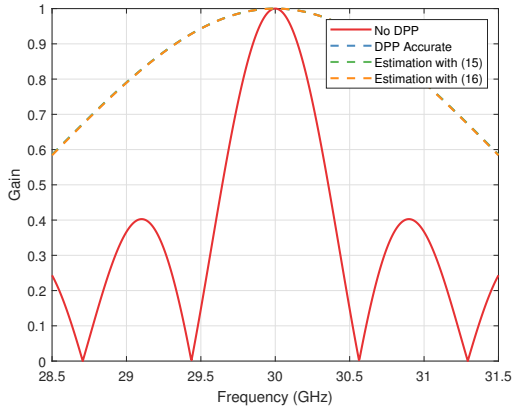

Fig. 5. Illustration of the beamforming gain with DPP architectures.

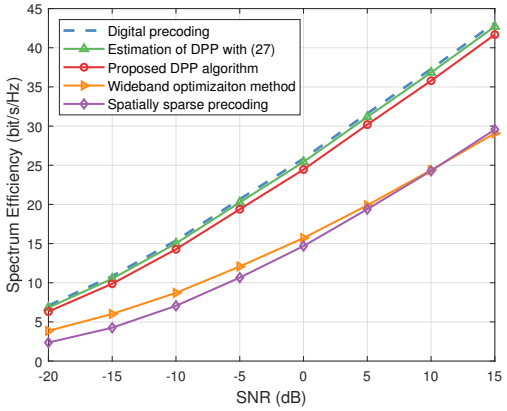

Fig. 6. Comparison on the spectrum efficiency over different SNRs.

$\mathbf{A}_{\mathrm{t},m}$ is a unitary matrix. Since $\mathbf{A}_{\mathrm{t},m}$ and $\widetilde{\mathbf{V}}_m$ are both unitary, when $\mathbf{F}_{\mathrm{A}}^{\mathrm{PS}}\mathbf{F}_{\mathrm{A},m}^{\mathrm{TTD}} = \mathbf{A}_{\mathrm{t},m}$ and $\mathbf{F}_{\mathrm{D},m} = \mathbf{F}_{\mathrm{D,m}}^{\mathrm{opt}}$ are satisfied, the maximum spectrum efficiency could be obtained.

However, due to the beam defocus effect in UCA systems, $\mathbf{F}_{\mathrm{A}}^{\mathrm{PS}}\mathbf{F}_{\mathrm{A},m}^{\mathrm{TTD}} = \mathbf{A}_{\mathrm{t},m}$ could not be perfectly obtained. Therefore, the key factor influencing the spectrum efficiency lies in the analog beamforming gain, which can be expressed as

$$\begin{aligned}&\left(\mathbf{F}_{\mathrm{A},m}^{\mathrm{TTD}H}\mathbf{F}_{\mathrm{A}}^{\mathrm{PS}H}\mathbf{A}_{\mathrm{t},m}\right)^{H}\mathbf{F}_{\mathrm{A},m}^{\mathrm{TTD}H}\mathbf{F}_{\mathrm{A}}^{\mathrm{PS}H}\mathbf{A}_{\mathrm{t},m}\\&=\mathrm{blkdiag}\left(\left[G_m^2(\mathbf{b}_{m,1},\phi_1),\cdots,G_m^2(\mathbf{b}_{m,N_{\mathrm{s}}},\phi_{N_{\mathrm{s}}})\right]\right).\end{aligned}\tag{26}$$

Noting that the beamforming gain $G_m(\mathbf{b}_{m,i},\phi_i)$ is independent of angles, the spectrum efficiency can be expressed as

$$\begin{aligned}R_m&\overset{(a)}{=}\log_2\left(\left|\mathbf{I}+\frac{\rho}{N_s\sigma_n^2}G_m^2(\mathbf{b}_{m,l},\phi_l)\mathbf{\Sigma}_m^2\right|\right)\\&\overset{(b)}{\approx}\log_2\left(\left|\mathbf{I}+\frac{\rho}{N_s\sigma_n^2}\,{}_1F_2\left(\frac{1}{2};1,\frac{3}{2};-\frac{a^2}{4}\right)^2\mathbf{\Sigma}_m^2\right|\right),\end{aligned}\tag{27}$$

where equation (a) is obtained due to the independence of G_m and ϕ_l and approximation (b) is derived from the conclusion in **Corollary 1**. A larger K will result in a smaller a, where the spectrum efficiency is expected to be further enhanced.

VI. Simulation Results

We consider a mmWave wideband communication system with central frequency $f_c = 30$ GHz and bandwidth $B = 3$ GHz. A 256-element UCA is equipped at BS to serve a single user equipped with a 4-element ULA.

The beamforming gain with 8 TTDs and without TTDs is plotted in Fig. 5. It can be seen that the introduction of TTD has significantly improved the beamforming performance compared with classical hybrid precoding. The green dashed line perfectly covers the blue and black lines, revealing that approximations in (15) and (16) achieve high accuracy.

The comparison of spectrum efficiency over different precoding algorithms with 16 TTDs is plotted in Fig. 6. The baselines include digital precoding, optimization-based method [8], and spatially sparse precoding [4]. It can be seen that (27) obtains accurate estimation, and DPP architecture outperforms optimization-based method and spatially sparse precoding and achieves about 95% performance of digital precoding. The reason lies in that the optimization-based method only aims to achieve a balanced beamforming gain across the bandwidth. Instead, DPP could generate frequency-dependent phase shifts, expected to obtain ideal beamforming gain at any frequency.

VII. Conclusion

In this paper, the mechanism of the beam defocus effect in UCA systems is investigated for the first time. The dispersed beam pattern in the angular and frequency domain are characterized, and the DPP architecture and corresponding precoding algorithm are introduced to mitigate the beam defocus effect in UCA systems. The discussions of multi-user MIMO communication scenarios are left for future research.

VIII. Acknowledgment

This work was supported in part by the National Key Research and Development Program of China (Grant No. 2020YB1807201), and in part by the European Commission through the H2020-MSCA-ITN META WIRELESS Research Project under Grant 956256.

References

[1] I. Ahmed, H. Khammari, A. Shahid, A. Musa, K. S. Kim, E. D. Poorter, , and I. Moerman, "A survey on hybrid beamforming techniques in 5G: Architecture and system model perspectives," *IEEE Commun. Surveys Tuts.*, vol. 20, no. 4, pp. 3060–3097, 4th Quart. 2018.

[2] L. Dai, J. Tan, Z. Chen, and H. V. Poor, "Delay-phase precoding for wideband thz massive MIMO," *IEEE Trans. Wireless Commun.*, vol. 21, no. 9, pp. 7271–7286, Sep. 2022.

[3] V. Kallnichev, "Analysis of beam-steering and directive characteristics of adaptive antenna arrays for mobile communications," *IEEE Antennas Propag. Mag.*, vol. 43, no. 3, pp. 145–152, Jun. 2001.

[4] O. Ayach, S. Rajagopal, S. Abu-Surra, Z. Pi, and R. W. Heath, "Spatially sparse precoding in millimeter wave MIMO systems," *IEEE Trans. Wireless Commun.*, vol. 13, no. 3, pp. 1499–1513, Jan. 2014.

[5] F. Bowman, *Introduction to Bessel functions*. North Chelmsford, U.K.: Courier Corporation, 2012.

[6] F. Zhang, W. Fan, and G. F. Pedersen, "Frequency-invariant uniform circular array for wideband mm-wave channel characterization," *IEEE Antennas Wireless Propag. Lett.*, vol. 16, pp. 641–644, Jul. 2017.

[7] Z. Wu and L. Dai, "The manifestation of spatial wideband effect in circular array: From beam split to beam defocus," *arXiv preprint arXiv:2305.02875*, May 2023.

[8] S. Park, A. Alkhateeb, and R. W. Heath, "Dynamic subarrays for hybrid precoding in wideband mmwave MIMO systems," *IEEE Trans. Wireless Commun.*, vol. 16, no. 5, pp. 2907–2920, May 2017.